Sustainable Chemical Engineering
http://ojs.wiserpub.com/index.php/SCE/

Research Article

Enhancing the Cu (II) Removal in Water Using Functional Hybrid Membranes

Noelle C. Zanini[1], Rennan F. S. Barbosa[1], Alana G. de Souza[1], Rafaela R. Ferreira[1], Paulo H. Camani[1], Sueli A. Oliveira[1], Daniella R. Mulinari[2], Derval S. Rosa[1*]

[1]Center for Engineering, Modeling, and Applied Social Sciences, Federal University of ABC, Santo André, Brazil
[2]Department of Mechanic and Energy, State University of Rio de Janeiro, Resende, Brazil
Email: dervalrosa@yahoo.com.br

Received: 24 January 2024; **Revised:** 3 April 2024; **Accepted:** 7 April 2024

Abstract: This work developed hybrid EIPS/NIPS membranes of poly (butylene adipate-co-terephthalate) (PBAT) with nanocurcumin (NC) and/or Cloisite 20A (C20A). The dispersed phases were characterized by dynamic light scattering (DLS), ζ potential, X-ray diffractometry (XRD), scanning electron microscopy (SEM), and fourier-transform infrared spectroscopy (FTIR), while XRD, SEM, FTIR, mechanical properties, contact angle, and copper sorption evaluated the composite membranes. DLS analysis indicated that the dispersed phases present a nanometric size distribution; ζ potential measurements showed low electrostatic stability, explaining the agglomeration effects observed. Pure PBAT membranes presented macro-pores throughout their structure, which showed a slight size reduction with the inclusion of NC and C20A. The membrane's mechanical performance was affected by the presence of the pores that functioned as stress-concentrating defects, and the inclusion of the dispersed phases increased the elastic modulus and tensile strength, especially for PBAT/0.5% C20A with values 18.7 and 8.9% higher than those of pure PBAT, respectively. Hybrid EIPS/NIPS membranes showed a hydrophilic nature with all the contact angle measurements lower than 90°. The sorption tests using a high-concentration copper solution (1,000 mg/L) showed a removal of around 25%. These results highlighted the development of new eco-friendly membranes using NC and C20A as dispersed phases with the potential to remove toxic elements from water.

DOI: https://doi.org/10.37256/sce.5220244351

Graphical abstract

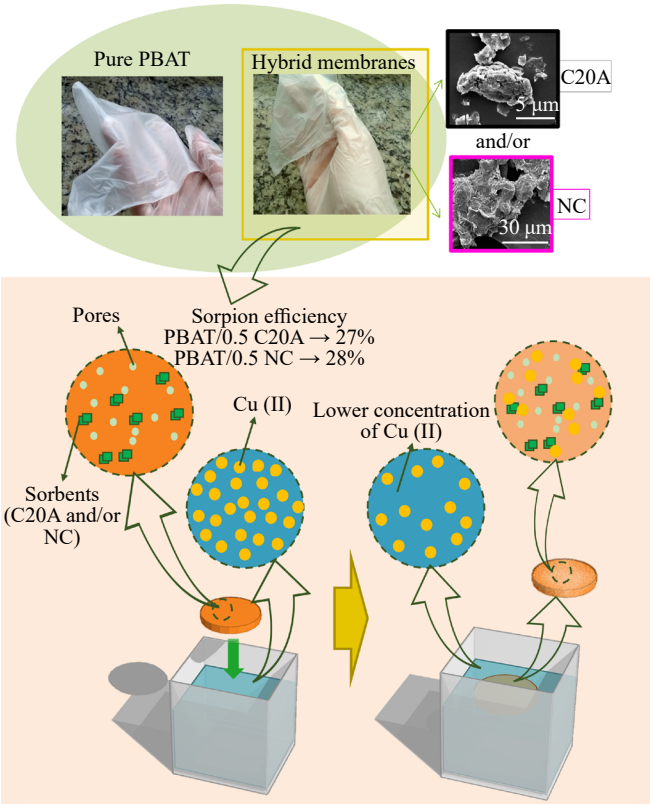

Keywords: membranes, water treatment, curcumin, cloisite 20A

1. Introduction

The presence of heavy metals in the environment is a global problem that poses severe threats to marine life and human health due to their toxicity, non-biodegradability, and bioaccumulation.[1-2] Heavy metals refer to elements with atomic densities above 4.5 g cm^{-3} and are derived from anthropogenic sources, such as petroleum, metal smelting, and electroplating.[3] A more up-to-date nomenclature can refer to heavy metals and other harmful elements as potentially toxic elements (PTEs) since, above a specific concentration, they can be harmful to the ecosystem and living organisms.[4] There are several PTEs related to anthropogenic activity, such as antimony (Sb), arsenic (As), beryllium (Be), cadmium (Cd), fluoride (F), gold (Au), lead (Pb), mercury (Hg), molybdenum (Mo), nickel (Ni), rubidium (Rb), selenium (Se), silver (Ag), uranium (U), vanadium (V), zinc (Zn), and copper (Cu).[5]

As a transition metal, copper can be found in nature in different oxidation states, such as a monovalent and bivalent ion, Cu (I) and Cu (II), respectively.[6] While Cu (I) is absorbed into the intestine through food intake, Cu (II) can originate from water sources and may not be absorbed, increasing the concentration of copper in the human organism.[7] Due to its industrial applications, Cu (II) can also be found in high wastewater concentrations. However, the permissible limit for copper ions in industrial effluents is reported as 1.3 and 2.0 ppm by the World Health Organization and USEPA, respectively.[8-9] Above these limits, the literature reports toxic effects on human health, such as carriers of the gene for Wilson disease, gastrointestinal effects,[10] metabolic disorders,[11] and even death.[10]

Over the last decades, different techniques have been used to remove PTEs, such as chemical precipitation,[12] ion exchange,[13] ion flotation,[14] coagulation/flocculation, osmosis, and electrochemical removal. However, these methods have disadvantages, such as erratic removal of metal ions, creation of toxic sludge, or high energy consumption,[15]

and, thus stimulate the search for cheaper and high-efficiency modern technologies. Among the PTE removal trends, adsorption is highlighted as a promising and efficient technique.[16] Few authors have reported combining the adsorption process in membranes, aiming for higher efficiency and metals removal selectivity, where sorbents can be used as fine particles to increase the interface area available for adsorption.[17-19] Several materials can be used to prepare the membranes, such as poly (vinylidene fluoride)/polyaniline, polyethylene, polyacrylonitrile, polyvinyl alcohol, and poly (N, N-dimethylacrylamide-co-2-hydroxyethyl methacrylate),[20] and also 2D materials such as boron nitride,[21] graphene[22] and MXene.[23] However, due to environmental concerns, biodegradable polymers, e.g., cellulose,[24] polylactic acid,[25] and polybutylene adipate-co-terephthalate,[26] have been widely used for membranes.

Inorganic adsorbents can remove PTEs from water, and the literature covers examples of inorganic-based adsorbents, such as layered double hydroxide,[27] metal-organic frameworks,[28] silica-based titanate,[29] and clays.[30-32] Montmorillonite (MMT) is a clay and one of the most studied inorganic materials for this application due to its high cation exchange capacity, natural electronegativity, controllable interlamellar spacing, and green and non-toxic properties.[33] The interlamellar space can be functionalized to enhance MMT potential application further and offer newly available interactions. The insertion of hydrogenated ammonium organic modifiers deserves a highlight since MMT modified with those modifiers is known as Cloisite.[34] Mohajeri and co-workers studied nano Cloisite Na^+ to remove Pb (II) and Cu (II), obtaining 40% and 16% adsorption efficiency, respectively.[31] Another type of Cloisite, the Cloisite® 20A, presents a potential application for heavy metal removal in wastewater, which has not been extensively explored in literature for Cu (II) removal. Although it is not commonly used to remove PTEs, justifications for using Cloisite® 20A can be found in the literature.[35]

Besides inorganic-based materials, organic-based materials such as cellulose,[36] natural fibers residues,[37] chitosan,[38] and curcumin[39] also can remove PTEs from aqueous media. Curcumin is a polyphenolic organic compound from turmeric (Curcuma longa) of formula $C_{21}H_{20}O_6$ and is a biomaterial little studied for this purpose but with great application capacity due to its symmetric molecular structure and terminations of hydroxyl and ketone functional groups.[40-41] Ferrari, Xi, and co-workers related that curcumin could have a strong chelation effect on metal ions.[42-43] Still, the complexes formed between curcumin-metal ions lack further investigation of their complexes' properties. Both clays and curcumins can be dispersed phases in polymeric matrix membranes to remove PTEs from contaminated water. Moradi and co-workers used boehmite clay particles modified with curcumin in poly (ether-sulfone) membranes obtained by phase inversion for retention of multiple bivalent ions such as Cu (II), where the addition of 0.5% loading of clay and curcumin combined decreased the content of the contaminants in water.[44]

According to Hashim and co-workers, hybrid materials are nanocomposites with at least one element at a nanoscale.[45] Therefore, this article is a follow-up to a previous study[35] and investigated the adsorption-hybrid membranes prepared using PBAT as a polymeric matrix, nanocurcumin (0.5% m/m), and nanoclay Cloisite® 20A (C20A (0.5% m/m) as sorbents, aiming their potential application in reducing PTEs concentration in wastewater. Besides, the efficacy of the hybrid EIPS/NIPS membranes was investigated in reducing the Cu (II) concentration in a solution simulating an industrial effluent.

2. Materials and methods

2.1 *Materials*

PBAT, commercially named Ecoflex® 87 F Blend C1200 density of 1.25 g cm^{-3} at 23 °C, (BASF SE, Germany), was supplied by BASF SE (São Paulo, Brazil). Chloroform (P.A.-ACS), sodium chloride (NaCl) (P.A.-ACS), ethyl alcohol (99, 5% of purity), copper nitrate II trihydrate ($Cu(NO_3)_2)\cdot 3H_2O$) (P.A.-ACS), and nitric acid (HNO_3) (70% of purity) were purchased from Synth (São Paulo, Brazil). The modified montmorillonite nanoclay BYK Cloisite® 20A Nanoclay (C20A) was purchased from Songhan Plastic Technology Co., Ltd. The turmeric powder (or fresh turmeric) derived from curcumin was purchased from a local supermarket (Jundiaí-SP).

2.2 *Methods*

Curcumin preparation:

Firstly, 40 g of turmeric powder was added to 200 mL of ethanol and kept under magnetic stirring for 1 h to obtain curcumin.[44] Then, the mixture was vacuum-filtered and dried at 30 °C for 24 h. Nano-sized curcumin (NC) structures were obtained by mechanical ball milling using a rotational mill (Model Q298, brand QUIMIS, 110 V, 60 Hz, 25 W, 150 rpm rotation on the drive roller). The grinding method was adapted from Jha and co-workers,[46] using a metal pot (300 mL) attached to a 1 L porcelain jar model 21 A (Chiarotti). 200 g of alumina beads (10 mm diameter) and 10 g of curcumin (ratio 20:1 m/m) were added to the metal pot. Before grinding, the curcumin was dried at 30 °C for 24 h. The milling process took place for 24 h at room temperature.

Polymer solution preparation:

A polymeric solution of PBAT 15 wt% in chloroform (85 wt%) was prepared under constant magnetic stirring for 6 h. A saturated aqueous sodium chloride (NaCl) solution (porogen with a volume corresponding to 6 wt% relative to the PBAT 47) was added. The mixtures were magnetically stirred for 30 min and then subjected to high-intensity ultrasound for 1 min (Sonics Vibra-cell VCX 500-VCX 750 sonicators) under the operating conditions: energy of 92,000 J and amplitude of 50%. The solutions with phase insertion of C20A and/or NC had an extra step in the mixing process before ultrasonication by adding the pre-set proportions of the dispersed phase(s), e.g., 0.5 wt% of C20A and/or 0.5 wt% NC. After adding the dispersed phase(s), the mixture was stirred for 1 h.

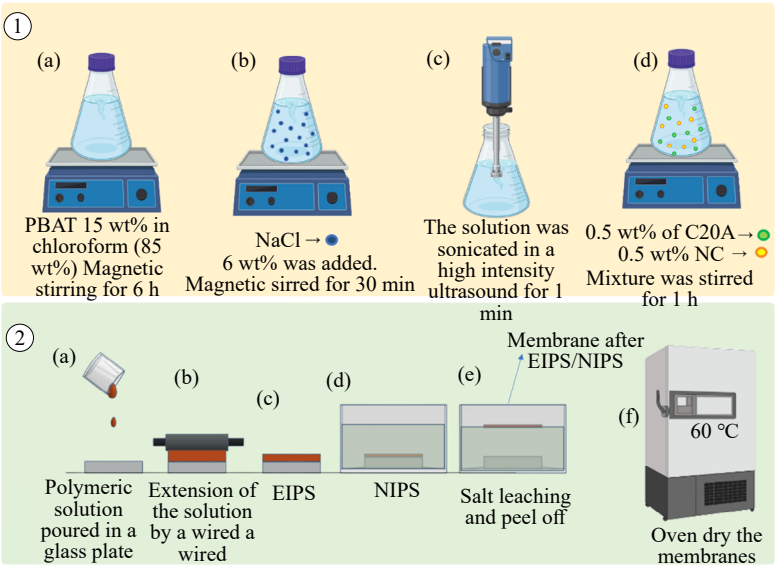

Figure 1. Illustrative scheme of methodology preparation for the functional hybrid EIPS/NIPS membrane, (1a-c) preparation of PBAT solution and (1d) PBAT membrane with C20A and/or NC loading; (2a-e) EIPS/NIPS membranes structure obtaining and (2f) the final drying step

Membrane preparation by EIPS/NIPS:

The polymer solution previously described (with porogen and with or without dispersed phase(s)) was applied to glass plates (13 × 18 cm) and spread out using a 200 µm Erichsen wire (200 µm). The procedure was done with 1 min drying time for partial solvent evaporation (EIPS). After evaporation, the plates were immersed in polyethylene trays in a non-solvent (NIPS) (distilled water) coagulation bath to induce phase separation. Then, the membranes were separated from the glass plates and remained in a distilled water bath for 24 h for salt leaching, with a subsequent dry process in an oven at 60 °C for 6 h.[47] The EIPS/NIPS membranes were obtained, as shown in Figure 1, and the compositions were based on a previous study[35] and the literature.[44] The composition of the polymer solution and dispersed phases (NC and C20A) are described in Table 1.

Table 1. Composition of EIPS/NIPS membranes developed, with the percentages of PBAT solution, C20A, and/or NC powders

Membrane	PBAT solution (%)	Cloisite® 20A (C20A) (%)	Curcumin (NC) (%)
PBAT	100.0	-	-
PBAT/0.5 C20A	99.5	0.5	-
PBAT/0.5 NC	99.5	-	0.5
PBAT/0.5 C20A + 0.5 NC	99.0	0.5	0.5

2.3 *Characterization*

2.3.1 *Dynamic light scattering (DLS) and ζ potential*

The Dynamic light scattering (DLS) recorded the average particle diameter of the adsorbents (C20A and NC). It was done with a stable 90° scattering angle using Zetasizer Nano-ZS (Malvern Panalytical Ltd., Malvern, U.K.). The adsorbents were prepared with 1 mL aliquots and diluted in 100 mL distilled water. The tests were done in triplicate. The ζ potential used the same equipment and sample preparation.

2.3.2 *X-ray diffractometry (XRD)*

The adsorbents (C20A and NC) and EIPS/NIPS membranes were analyzed by X-ray diffraction measurements using a D8 Focus diffractometer (Bruker AXS Advanced X-ray Solutions GmbH, Karlsruhe, Germany), operating at 40 kV and 40 mA. It used monochromatic CuKα radiation (λ = 1.54056 Å) at a step width of 0.01° and counting time of 100 s at each 0.5°, from 2θ = 10° to 60°.

2.3.3 *Scanning electron microscopy (SEM)*

The adsorbents (C20A and NC) and EIPS/NIPS membrane samples (surface and cross-section) were coated with a 25 nm thick gold layer using Sputtering Leica EM ACE 200 (Leica Microsystems, Wetzlar, Germany). The cross-section membrane samples were obtained by fracturing the membrane after nitrogen immersion. Micrographs were performed using a microscope FEI Quanta 250 (Thermo Fisher Scientific, Hillsboro, Oregon, USA), using an accelerating voltage of 10 kV and a spot size of 4 nm.

2.3.4 *Fourier-transform infrared spectroscopy*

The adsorbents (C20A and NC) and EIPS/NIPS membranes were analyzed by Fourier-transform infrared spectroscopy (FTIR) using a Frontier 94.942 (PerkinElmer Inc, Massachusetts, USA) with attenuated total reflectance (ATR) mode in a range of 500-4,000 cm^{-1}, 32 scans, and spectral resolution of 4 cm^{-1}.

2.3.5 *Mechanical testing*

Tensile tests analyzed the EIPS/NIPS membranes using an Instron 3367 (Instron®, USA Norwood, USA). All experiments were conducted according to the ASTM D638-14 standard. Five specimens were evaluated with a load cell of 50 N and 50 mm min^{-1} test speed.

2.3.6 *Contact angle (CA)*

The EIPS/NIPS membranes were analyzed by contact angle using a dynamic contact angle tensiometer (SEO) model Phoenix 300 (Kromtech Alliance Corp., London, UK), with three phases (air/water/sample). The static contact angles (θ_{est}) were determined according to the Young-Laplace equation by observing a water droplet of 4.00 µL deposited on the membrane surface. The contact angle values were collected in triplicates for 5 minutes, in 3-second intervals of each measurement, and a mean value of the collected values was considered.

2.3.7 *Copper adsorption*

A Cu (II) solution containing 1,000 ppm of Cu (II) was prepared to simulate the effluent from a plating industry for the adsorption experiments.[48] $Cu(NO_3)_2 \cdot 3H_2O$ was dissolved in a solution of 0.01 M HNO_3, and a sodium hydroxide solution of 0.01 M NaOH was used for pH 5 correction. The pH was set to 5 due to precipitation and low stability of aqueous solutions with pH > 5.[49] Once the solution was prepared, 0.1 g of each EIPS/NIPS membrane was placed in a plastic tube and mixed with 50 mL of Cu (II) solution, on the other hand, an adsorbent dosage of 2 g/L.[50] Adsorption measurements in triplicate were performed from the beginning (t = 0) and at times (t) of 10 min, 45 min, and 1,440 min.

Evaluation of Cu (II) concentration for adsorption occurred using Cary 50 UV-vis spectrophotometer (Varian) at the wavelength of 305 nm for Cu (II).[51-52] The adsorption efficiency was calculated using Equation 1, where C_o (mg/L) is the initial concentration of the metal ion in the wastewater before adsorption, and C_f (mg/L) is the final concentration of the metal ion in the wastewater after adsorption.

$$\text{Efficiency}\% = \frac{C_o - C_f}{C_o} \times 100\% \quad (1)$$

3. Results and discussion

3.1 *Dynamic light scattering (DLS) and ζ potential*

Dynamic light scattering (DLS) was used to evaluate the distribution profile and hydrodynamic radius (RH) of C20A and NC, considering these nanomaterials to be spheres. The C20A showed a trimodal distribution profile (Figure 2), with average peak values around 10.1, 342, and 5,560 nm, indicating a polydisperse and heterogeneous sample. The first two peak values are characteristic of nanoclays, as reported in the literature, while the higher radius values (5,560 nm) indicate lamellae agglomerations due to van der Waals bonds. According to Zdiri and co-workers, although individual nanoclays have nanometric dimensions, MMT aggregates have micrometric dimensions, between 0.1-10 μm, consisting of lamellae in random directions.[53] The presence of agglomerates justifies using low C20A contents in the membranes, aiming to achieve better dispersion and adequate performance for application in water treatment.

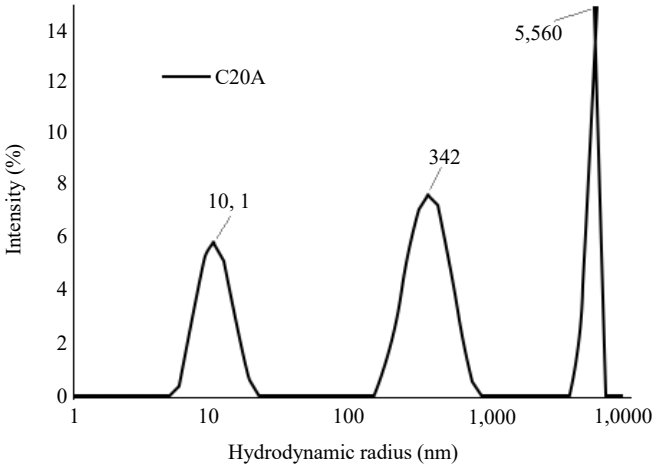

Figure 2. Distribution profile and hydrodynamic radius (RH) of C20A

The nanocurcumin DLS results showed a broad peak, and the wide distribution is associated with the mechanical grinding process that results in irregularly shaped and amorphous particles.[54] It was observed that two peaks were located at 255 and 4,150 nm. The ball milling process is a top-down mechanical method of green synthesis that allows the conversion of microparticles into nanometric dimensions,[55] as observed in Figure 3.

The ζ potential was used to evaluate the electrostatic stability of the nanoparticles, and the samples showed ζ potential values of -11.5 and -3.2 mV for C20A and NC, respectively. According to the literature, particles with high ζ potential values in the module present higher electrical stability, while particles with lower ζ potential could present agglomeration tendency.[56] Since the dispersed phases have low ζ potential, they can present agglomeration effects, corroborated by DLS results, with C20A lamellae clusters and poor NC dispersion.

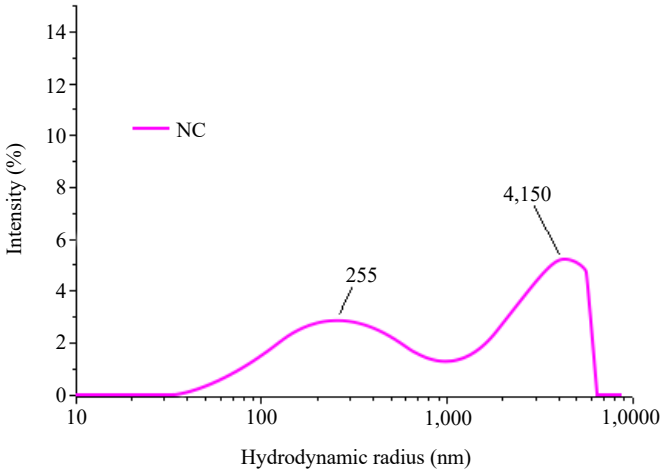

Figure 3. Distribution profile and hydrodynamic radius (RH) of NC

3.2 *X-ray diffractometry*

The XRD technique was used to determine the materials' crystalline pattern, and Figure 4 shows the obtained diffractograms.

C20A showed two broad peaks between 2θ = 0-10°, at i) 3.6° and ii) 7.1°, where peak i) refers to the crystallographic plane (001), and peak ii) refers to the crystallographic plane (002).[57] The peak i) showed an interplanar distance (d) of 24.2 Å and is assigned to the montmorillonite-modified layers,[58-61] corroborating the organomodified nature of Cloisite® 20A. The peak ii) showed d = 12.4 Å, associated with the layers that did not suffer the influence of the organic modifier.[62] Other peaks resulting from the modification of MMT were also seen at iii) 19°, iv) 24° and v) 35°[63] (Figure 4a). According to Patiño-Soto and co-workers, the peak at 3.6° (Figure 4b) is the most characteristic for organomodified clays, corresponding to the original basal reflection peak for Cloisite® 20A.[64] Abdolrsaouli and co-workers reported the second peak of Cloisite® 20A at 8.2°, reflecting the smaller interplanar distance, i.e., more excellent packing of the MMT layers.[59] The crystallinity index (CI) of the C20A was 85.6%, which agrees with literature reports.[65]

Figure 4c and d-e demonstrate the curcumin XRD patterns before and after the milling process, respectively. Figure 4c shows a broad band with two peaks at 17.4 and 22.1°, highlighting the amorphous characteristics of curcumin associated with the turmeric organic nature.[66] After the mechanical milling (Figure 4d-e), the amorphous character of the sample was accentuated due to the ball grinding friction.[67] In the nanometric particles, there is an increase in surface defects and random bonds to facilitate adsorption, as illustrated in Figure 4f.[68] Zhang and co-workers reported an amorphization of curcumin nanoparticles milled for 24 h at 157 rpm.[54] According to Qiu and co-workers, the mechanical energy in the grinding process can disorganize crystalline areas and result in amorphization, increasing samples' adsorption capacity due to increased particle surface area.[69] However, the agglomeration process can mask the decrease in particle size after long grinding times.[70] The authors reported that the relationship between amorphization and particle agglomeration still requires further studies to understand the linkage of factors. Other authors reported increased particle sorption capacity after amorphization.[71-73]

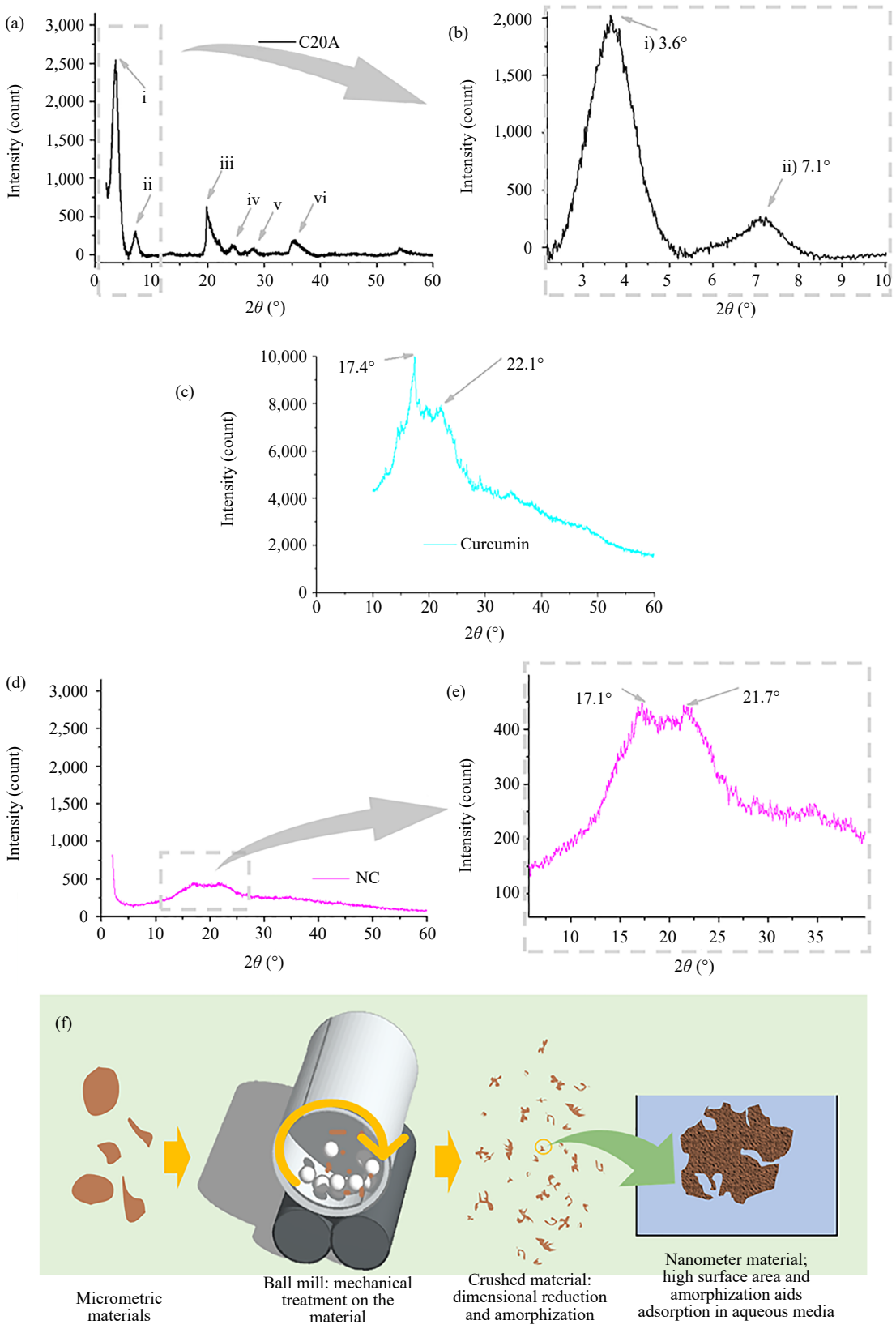

Figure 4. Diffractometer patterns relating to C20A at (a) 2θ = 0-60°, and (b) zoom showing the 2θ = 0-10° region, (c) unground curcumin, and to NC at (d) 2θ = 0-60° and zoom at (e) 2θ = 3-38°, (f) illustrates the mechanical grinding of curcumin

The lack of atomic periodicity of adsorbent materials also influences diffusion processes involving adsorption.[74] The NC diffractometric profile is like the nanometric curcumin well presented in the literature.[75-76] Joly and Latha identified a broad band centered at $2\theta = 17°$,[77] which was used to calculate the CI value of 30.6% in this work.

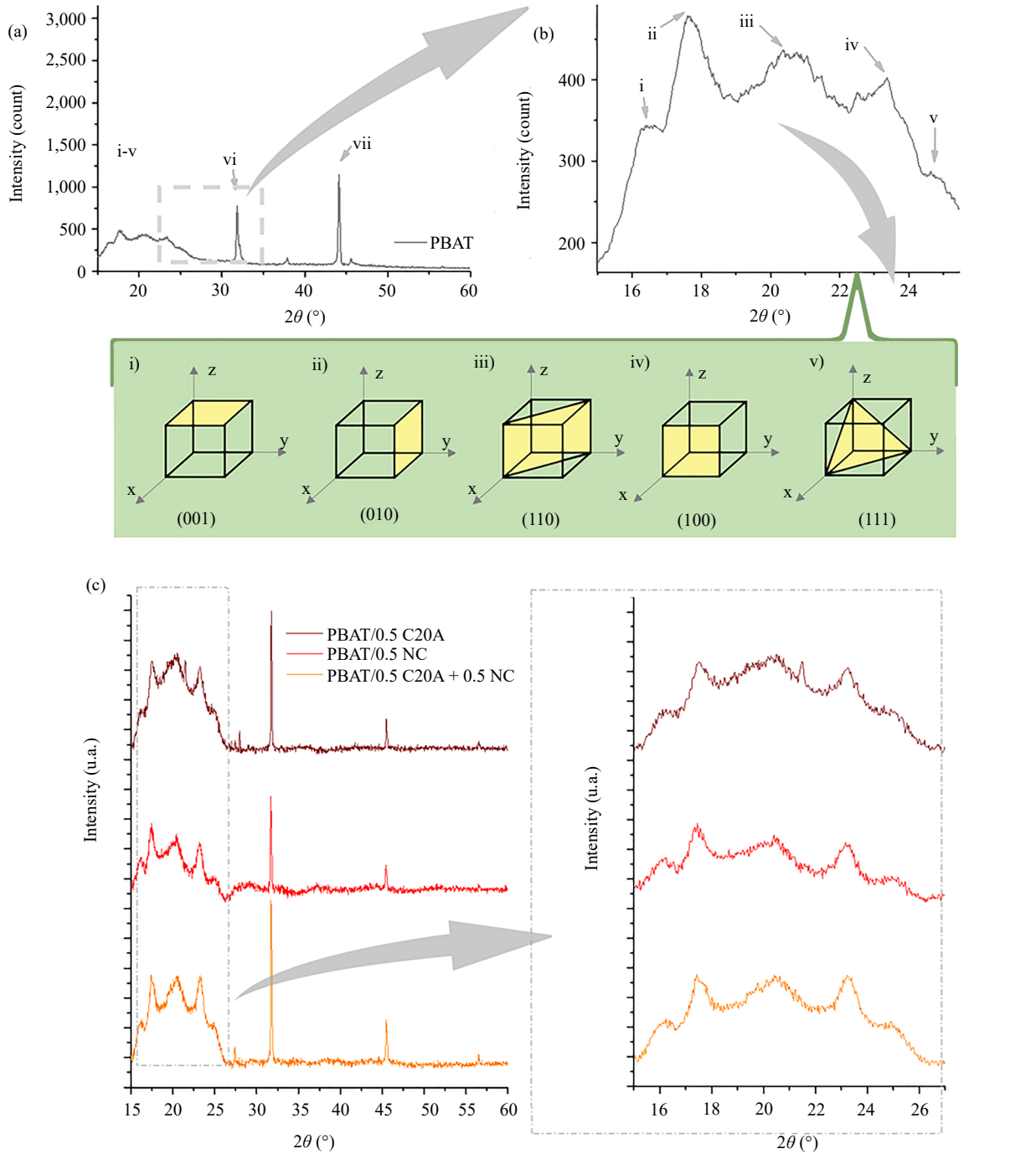

Figure 5. Diffractometer pattern for (a) pure PBAT membrane, (b) zoom for better visualization between 10-26°, and graphical representation of the Miller Indices. (c) hybrid EIPS/NIPS membranes ($15° < 2\theta < 60°$) and zoom for best visualization 15-27°

The XRD was also used to investigate the developed EIPS/NIPS membranes, as shown in Figure 5.

Figure 5a shows a standard PBAT diffractogram with characteristic peaks between 2θ = 15-25° (Figure 5b, reflections from i to v).[78-81] Kashi and co-workers described that the peaks in the mentioned range correspond to the characteristic peaks of the PBAT due to the basal reflections in the Miller index planes 2θ = 16.3° (001), 2θ = 17.6° (010), 2θ = 20.3° (110), 2θ = 23.3° (100), and 2θ = 24.6° (111). Figure 5c shows the XRD patterns of the membranes, which showed high similarity with the pure polymer.

The diffractograms with lower peak intensity in the hybrid EIPS/NIPS membranes show more excellent exfoliation of C20A and dispersion of NC along the membrane weight, despite the tendency to agglomerate seen in DLS and ζ potential. The nanometer size of C20A may facilitate the dispersion and interface reinforcement/matrix, influencing the crystallinity and enabling a more outstanding adhesion of the nanoparticles of PBAT films for better mechanical properties.[82-83]

3.3 *Scanning electron microscopy*

The micrographs obtained by SEM of the surface and cross-section of EIPS/NIPS membranes are shown in Figure 6.

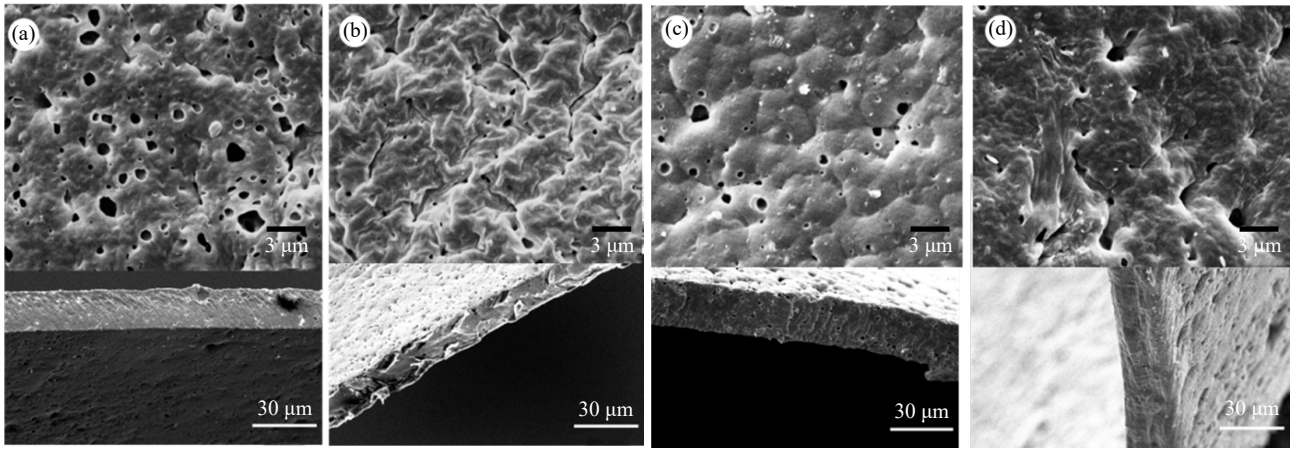

Figure 6. SEM micrographs of EIPS/NIPS membranes surface: (a) PBAT, (b) PBAT/0.5 C20A, (c) PBAT/0.5 NC, and (d) PBAT/0.5 C20A + 0.5 NC

The results demonstrated that the surface of the pure PBAT membrane presents pores with a more homogeneous cross-section (less surface roughness) than the hybrid membranes. For PBAT/0.5 C20A, it was noted that adding nanoclay decreases the pore diameter by changing the surface, leaving it more irregular and its cross-section, while for PBAT/0.5 NC, the surface becomes less rough. Such differences between the dispersions of the phases may result from different interactions with the matrix since C20A tends to exfoliate when in polymer solutions. The PBAT/0.5 C20A + 0.5 NC sample has more evidence of a dispersed phase due to its irregularity, agglomerations, and higher additive fractions.

Table 2 shows the average diameter and maximum pore size measurements of the EIPS/NIPS membranes and the average dry thickness measurements (cross-section after rupture).

Table 2. Average (µm) and maximum pore size (µm); and EIPS/NIPS membranes cross-sectional thickness (µm) (dry thickness)

Membrane	Average pore size (µm)	Max. pore size (µm)	Transversal section (µm)
PBAT	0.6 ± 0.5	4.6	22.9 ± 0.6
PBAT/0.5 C20A	0.5 ± 0.2	1.7	15.4 ± 1.2
PBAT/0.5 NC	0.5 ± 0.4	2.7	23.6 ± 1.5
PBAT/0.5 C20A + 0.5 NC	0.4 ± 0.3	2.0	26.5 ± 0.7

Compared to pure PBAT, all hybrid EIPS/NIPS membranes showed smaller average pore diameters ranging from 0.4 to 0.5 µm. Barbosa and co-workers obtained pores ranging from 0.25 to 0.6 µm in PBAT membranes with 6% NaCl as porogen.[84] The pores of the membranes for both preparation methods are classified as macropores because they exceed the size of 50 nm (according to the standard of the International Union of Pure and Applied Chemistry (IUPAC)).[85] Although PBAT/0.5% C20A membrane has lower dry thickness than pure PBAT (15.4 and 22.9 µm, respectively), most EIPS/NIPS membranes have thicknesses above 21 µm. According to Liu and co-workers, Young's modulus and tensile strength limit depend on a membrane's thickness.[86] Lima and co-workers observed that increasing the thickness of elastomeric membranes decreased both the wettability seen by the contact angle and the hardness of the membranes.[87]

3.4 *Fourier-transform infrared spectroscopy*

The FTIR analysis was also used to investigate the developed EIPS/NIPS membranes, and the obtained spectra are presented in Figure 7.

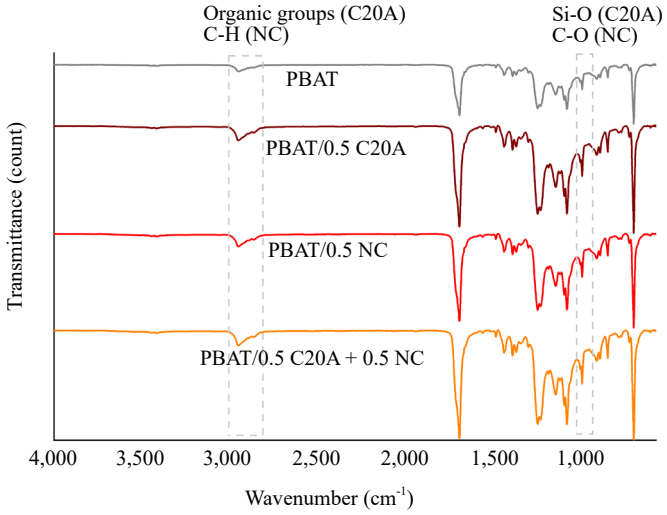

Figure 7. FTIR spectra EIPS/NIPS membranes, highlighting the prominent peaks associated with C20A and NC

The prominent peaks associated with PBAT structure are observed at 3,065 cm^{-1} (C-H stretching), 2,958, 2,875 cm^{-1} (CH_3 and CH_2 stretching), 1,710 cm^{-1} (C = O bond of ester group), 1,410 cm^{-1} (bending mode of O-CH_2), 1,366 cm^{-1} (bending mode of CH_2), 1,267 cm^{-1} (C-O group) and 726 cm^{-1} (deformations of the benzene ring). All EIPS/NIPS membranes presented these characteristics peaks.[88-89]

Regarding the hybrid EIPS/NIPS membranes, the bands found for NC are commonly observed at 3,312 cm^{-1} (OH stretching of the phenolic group), 2,920-2,851 cm^{-1} (C-H stretching), 1,638 cm^{-1} (C = C and C = O stretching), 1,241 cm^{-1} (angular deformation in the C-O-C plane), 1,101 cm^{-1} (C-O stretching), and 1,018 cm^{-1} (C-O-C stretching).[90-92] The bands corresponded to the chemical composition of phenolic groups for NC,[93] and these bands are essential for the sorption process of contaminant metal cations, as they can complex bivalent cations due to the direct binding of curcumin molecule with the ion or by hydrogen bond formation.[94] For C20A, the prominent peaks are observed at 3,632 cm^{-1} (O-H stretching), 2,921, 2,849 and 1,475 cm^{-1} (C-H stretching of alkylammonium groups), 1,639 cm^{-1} (O-H angular deformation), 1,004 cm^{-1} (Si-O vibration), 917 cm^{-1} (Al-OH-Al deformation) and 725 cm^{-1} (Si-O stretching).[95-96] Similarly, the silicates, aluminate, and alkylammonium groups are relevant to promote the complexation and removal of contaminants. The peaks of C20A and NC can be seen in Figure 8.

Comparing the FTIR spectra of hybrid EIPS/NIPS membranes, it was observed that they were mainly related to PBAT typical peaks, which could be attributed to i) the overlapping of some peaks of PBAT that are observed in similar regions of those from NC and C20A; ii) the low concentration of NC and C20A used in the membrane's formulation.

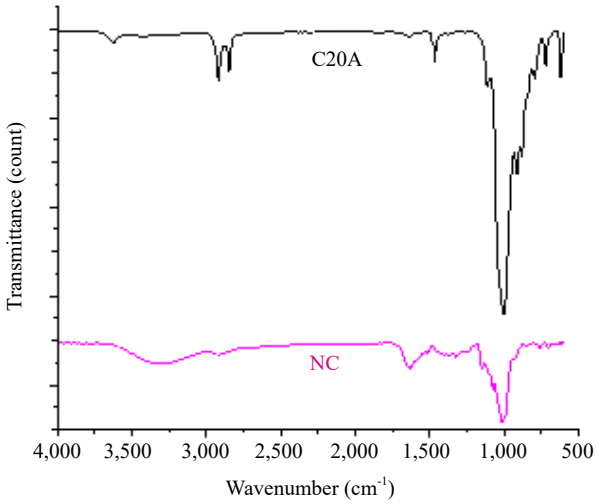

Figure 8. FTIR spectra of C20A and NC

3.5 *Mechanical testing*

The mechanical test was employed to investigate the mechanical properties of EIPS/NIPS membranes (Figure 9).

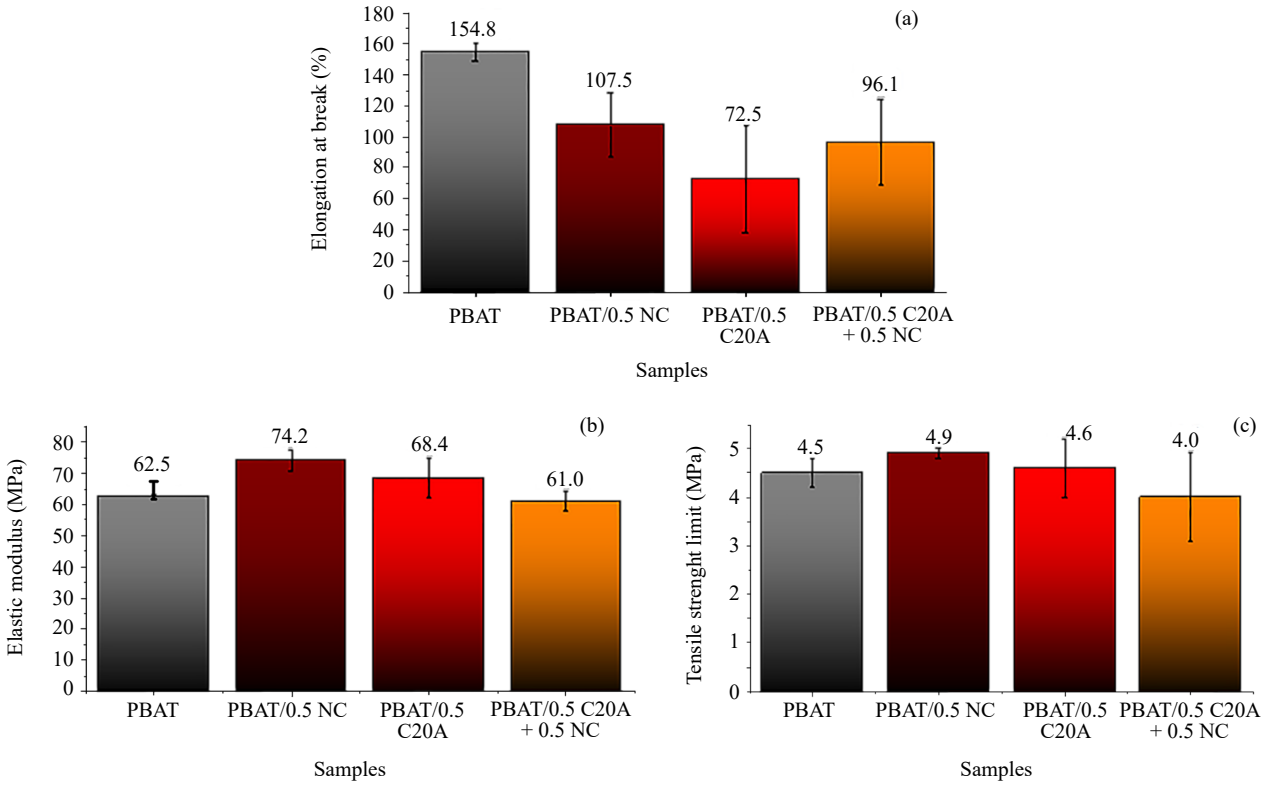

Figure 9. Mechanical properties of pure PBAT and hybrid EIPS/NIPS membranes, being (a) elongation at break (%), (b) elastic modulus (MPa), and (c) tensile strength limit (MPa)

The strain of a membrane is the elongation at break (%), which measures the flexibility, i.e., the ability of the film

to deform before cracking and eventual rupture.[97] In Figure 9a, it was observed that the pure PBAT membrane obtained the highest elongation at break (154%). In the literature, the elongation at break for PBAT is higher, with records of up to 508%.[98] The hybrid EIPS/NIPS membranes are smaller, which is associated with the fact that it is a porous membrane that may have affected the deformation since the pores may have acted as stress-concentrating defects that facilitate rupture.[47] The dispersed phase can reinforce the PBAT structure, increasing its rigidity and reducing the membrane's elongation. Both C20A and NC influenced this property, and among the hybrid EIPS/NIPS membranes, the one with the highest strain was PBAT/0.5 C20A (107.5%), and the lowest value was for the PBAT/0.5% NC membrane (72.5%). Thus, PBAT/0.5 C20A + 0.5 NC had an intermediate value compared to membranes with only one dispersed phase (96.1%).

A polymer's stiffness is determined by the elastic modulus, obtained by the slope of the linear portion of the stress-strain distribution for a polymer under compression. It is a widely popular metric for choosing materials with superior mechanical attributes. Figure 9b shows that membranes with only one dispersed phase added had a higher elastic modulus. Correia and co-workers also observed this behavior in PBAT membranes with charcoal addition, showing that adding dispersed phases increased membrane integrity.[97] In this work, compared to pure PBAT elastic modulus of 62.5 MPa, PBAT/0.5 C20A had an increase of 18.72% (74.2 MPa), and PBAT/0.5 NC had an increase of 9.44% (68.4 MPa). This fact corroborates the increase in IC seen in the XRD analysis, which increases the membrane's stiffness.

In Figure 9c, it was observed that the insertion of C20A in the PBAT/0.5 C20A (with 4.9 MPa) was the one that most favored the increase in tensile strength (8.9%) when compared to that of pure PBAT (4.5 MPa), followed by the PBAT/0.5 NC (4.6 MPa). Crystalline particle loading in polymeric matrix increases the stiffness of materials and thus can influence their tensile strength.[97] The PBAT/0.5 C20A + 0.5 NC membrane, on the other hand, showed no increase and had the lowest tensile strength limit (4.0 MPa), which may be an indication that both dispersed phases (C20A and NC) in the matrix did not favor the matrix/reinforcement interaction. Ludwiczak and co-workers studied the mechanical behavior of MMT in a PBAT and PLA polymeric matrix. The authors concluded that the role of clay as an active interfacial modifier in a polymeric composite still needs further research to understand the effect of the dispersed phase on material stiffness and deformation. Thus, the insertion of C20A and NC both separately and simultaneously is still a research object that is not fully understood.[98]

3.6 *Contact angle*

The contact angle (CA) is an essential measurement to investigate the surface behavior of the EIPS/NIPS membranes and their interaction with water. Figure 10 shows the dynamic CA over 5 min (Figure 10a), the representation of different CA classifications (Figure 10b), and the average CA (Figure 10c).

The dynamic measurement of the CA can investigate the interaction of the water droplet with the membrane surface as a function of time. Figure 10a showed that EIPS/NIPS membranes decreased in CA over the test time (5 min). It was also observed that CA values were lower than 90° throughout the assay. As illustrated in Figure 10b, hydrophilic materials have CA surfaces less than 90°, and hydrophobic materials have CA above 90°. Therefore, the EIPS/NIPS membranes obtained are hydrophilic.[99] That behavior was expected due to the hydrophilic nature of the biopolymer PBAT. Yasin and co-workers observed that the water droplet on poly (vinyl alcohol) membranes with chitosan particles exhibited a decrease in CA concerning time, i.e., the biopolymer matrix surface with a dispersed phase exhibits a hydrophilic nature.[100] Lin and co-workers also observed decreased CA with time for a polyhydroxybutyrate (PHB)/PBAT membrane.[101] Furthermore, the porous surface of the EIPS/NIPS membranes seen in the SEM micrographs may have reduced CA.[102]

Nevertheless, the dispersed phases' insertion influenced the membrane's CA. The average values of CA in Figure 10c demonstrated that pure PBAT has CA = 55.9°. Botta and co-workers found a CA of 55° for PBAT membranes, like this work. However, the authors observed that the insertion of biochar into the PBAT matrix increased the CA, increasing hydrophobicity,[103] unlike what occurred for the dispersed phases of this work, as seen in Figure 10c. The 0.5% C20A and/or NC loading was sufficient to decrease the CA. The EIPS/NIPS membranes with one dispersed phase had the lowest CA's, with PBAT/0.5 NC with CA = 46.5° and with prominence for PBAT/0.5 C20A with CA = 37.9°. Although both curcumin[104] and organomodified Cloisites[105] are hydrophobic, in the literature, it has already been discussed that both unmodified and modified MMTs, such as Cloisite,[106-107] and curcumin-based materials[108] can increase the hydrophilic character of polymeric films. Therefore, the insertion of nanoparticles may have increased

the surface roughness by increasing the surface capillary action and, consequently, the interaction with water.[109] This behavior of composite membranes may favor the application of the membranes for adsorption and filtration. In the case of PBAT/0.5 C20A + 0.5 NC, the CA = 54.4° was similar to the pure PBAT membrane, showing that the interaction of this hybrid EIPS/NIPS membrane surface with the aqueous medium is negatively affected by the simultaneous action of the dispersed phases.

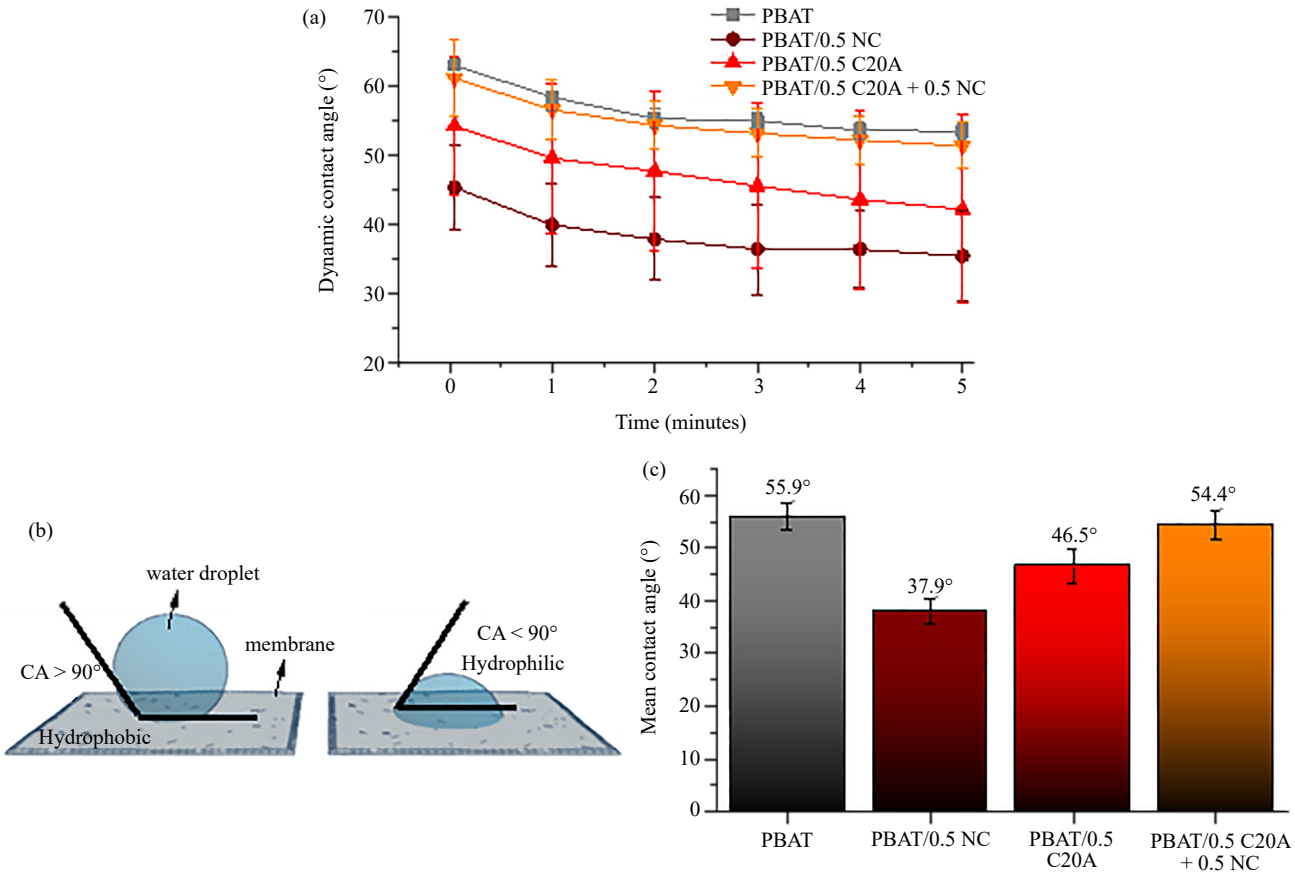

Figure 10. (a) Dynamic contact angle for the EIPS/NIPS membranes in the range of 0 to 5 min, (b) representation of a water droplet in a hydrophilic and a hydrophobic surface, and (c) mean values of the contact angle of the membranes

3.7 *Copper adsorption*

The adsorption test performed on the EIPS/NIPS membrane demonstrates the ability of the membrane to be an adsorbent material having a highly concentrated solution of contaminant, simulating the industrial effluent from a plating industry and the leak from the Brumadinho disaster (~ 1,000 mg/L).[48,110] Figure 11 shows the sorption efficiency (%) aiming to decrease the initial concentration of 1,000 mg/L of Cu (II).

Figure 11 demonstrated that the EIPS/NIPS membrane could decrease the contaminated solution's initial concentration. The times studied showed variation in efficiency up to 24 h. The pure PBAT membrane, e.g., showed an efficiency of 20.5% in 10 min and 21.2% in 24 h, i.e., an increase of only 3.4%. The minor variation in sorption efficiency may be due to the saturation of the monolayer of the EIPS/NIPS membranes surface in contact with a solution of high Cu (II) concentration, reaching maximum adsorption.[111]

The hybrid EIPS/NIPS membranes improved sorption efficiency, with membranes with only one dispersed phase being the most prominent in sorption efficiency at the end of the analysis (24 h), in the following order PBAT/0.5% NC (28.0%) > PBAT/0.5% C20A (27.0%) (Figure 11). Gaikwad and co-workers achieved a 27% removal efficiency of Cu

(II) from mining wastewater at pH 5.[112] In the case of the PBAT/0.5 C20A + 0.5 NC, no increase in adsorption efficiency was observed, having diminished their adsorption efficiency from T1 to T3 (24.4% to 16.7%, respectively). Thus, between 10 min and 24 h, there was a 31.5% reduction in efficiency. The literature addresses that the interaction of the material with the solution containing the PTE may initially saturate the adsorption sites and cause the sorption efficiency to be reduced by breaking bonds that interact with the contaminant.[113-114] Xu and co-workers observed a 17% drop in Cu (II) sorption efficiency due to the breaking of active sites of chitosan in contact with contaminated industrial effluent.[113] Karimi obtained a similar adsorption efficiency to this work using $Ca(OH)_2$, with a 20% removal efficiency of Pb (II) at pH 6 from industrial wastewater.[115] Kumar and co-workers mentioned a 10% and 20% removal efficiency of Cu (II) and Ni (II) in contaminated water using Trien.[116]

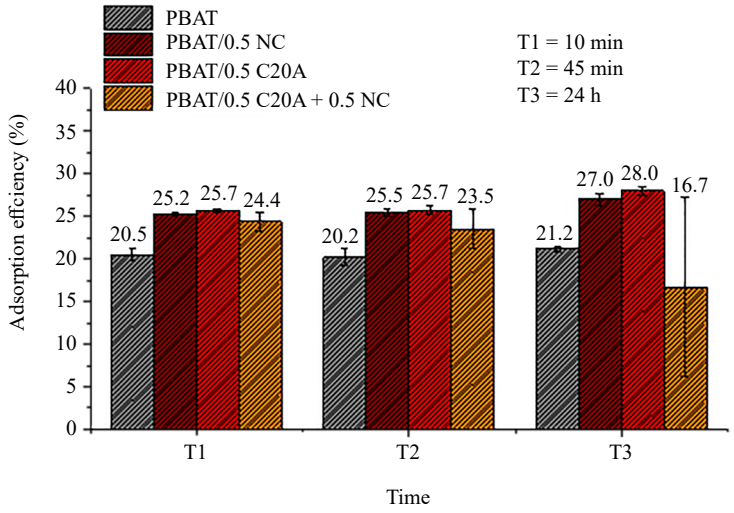

Figure 11. Sorption efficiency (%) of the adsorption tests of the membranes at times T1 = 10 min, T2 = 45 min, and T3 = 1,440 min

Therefore, the results are attractive since they illustrate the potential application of hybrid EIPS/NIPS membranes for removing PTEs, for which the inclusion of NC and C20A showed a potential to increase the membrane's potential. Additionally, using eco-friendly materials is appealing to reduce environmental impacts and promote sustainable treatment alternatives to increase water quality.

4. Conclusion

This work proposes the development of poly (butylene adipate-co-terephthalate) (PBAT) membranes with the inclusion of nanocurcumin (NC) and Cloisite® 20A (C20A) for the removal of toxic contaminants from water. Both dispersed phases presented nanometric size but with agglomeration effects observed due to their low ζ potential. C20A showed a crystallinity index (85.6%), while NC presented amorphization due to mechanical milling. The hybrid EIPS/NIPS membranes showed smaller pores, also impacting the membrane's mechanical performance, with the C20A promoting an increase in elastic modulus and tensile strength. In contrast, the PBAT/0.5 C20A + 0.5 NC showed reduced properties due to the amorphous nature of NC. EIPS/NIPS membranes present a hydrophilic nature, which is attractive for water contact applications. The sorption results showed that the membranes effectively reduced copper concentration even at low contact time, removing 25.7% for the PBAT/0.5 NC and 25.2 for PBAT/0.5 C20A. Thus, the PBAT/0.5 C20A + 0.5 NC membrane demonstrated a reduction in efficiency over time. The significant reduction in initial high concentration highlights the membrane's capability to eliminate toxic elements from water. Moreover, these findings emphasize using eco-friendly materials for water decontamination, providing a promising substitute for conventional treatment approaches. With the results obtained in this work, in future work in Cu (II) adsorption experiments using

C20A and NC in EIPS/NIPS membranes with PBAT matrix, other variables can be evaluated, such as adsorbent amount (NC and C20A alone or simultaneously) and Cu (II) solution concentration.

Acknowledgment

This research was funded by CNPq (308053/2021-4 and 403934/2021-4) and FAPESP (2022/01382-3, 2021/14714-1, 2021/08296-2, 2020/13703-3 and 2019/16301-6). The authors thank the UFABC, CAPES (Code 001), REVALORES Strategic Unit, CAPES (001), and Multiuser Central Facilities (CEM-UFABC).

Conflict of interest

The authors declare no competing financial interest.

References

[1] Kuang, Y.; Zhang, Z.; Wu, D. Synthesis of graphene oxide/polyethyleneimine sponge and its performance in the sustainable removal of Cu (II) from water. *Sci. Total Environ*. **2022,** *806*, 151258.
[2] Xiang, H.; Min, X.; Tang, C. J.; Sillanpää, M.; Zhao, F. Recent advances in membrane filtration for heavy metal removal from wastewater: A mini review. *J. Water Proc. Engineering* **2022,** *49*, 103023.
[3] Chen, R.; Zhang, Q.; Chen, H.; Yue, W.; Teng, Y. Source apportionment of heavy metals in sediments and soils in an interconnected river-soil system based on a composite fingerprint screening approach. *J. Hazard. Mater*. **2021,** *411*, 125125.
[4] Pourret, O.; Hursthouse, A. It's time to replace the term "heavy metals" with "potentially toxic elements" when reporting environmental research. *Int. J. Environ. Res. Public Health* **2019,** *16*, 4446.
[5] Ramanayaka, S.; Vithanage, M.; Sarmah, A.; An, T.; Kim, K. H.; Ok, Y. S. Performance of metal-organic frameworks for the adsorptive removal of potentially toxic elements in a water system: A critical review. *RSC Adv*. **2019,** *9*, 34359-34376.
[6] Mohajeri, P.; Smith, C. M. S.; Chau, H. W.; Lehto, N.; Azimi, A.; Farraji, H. Adsorption behavior of Na-bentonite and nano cloisite Na^{+} in interaction with $Pb(NO_3)_2$ and $Cu(NO_3)_2{\cdot}3H_2O$ contamination in landfill liners: optimization by response surface methodology. *J. Environ. Chem. Eng*. **2019,** *7*, 103449.
[7] Hsu, H. W.; Bondy, S. C.; Kitazawa, M. Environmental and dietary exposure to copper and its cellular mechanisms linking to alzheimer's disease. *Toxicol. Sci*. **2018,** *163*, 338-345.
[8] Awual, M. R.; Hasan, M. M.; Khaleque, M. A.; Sheikh, M. C. Treatment of copper (II) containing wastewater by a newly developed ligand based facial conjugate materials. *J. Chem. Eng*. **2016,** *288*, 368-376.
[9] EPA, U. S. *Edition of the Drinking Water Standards and Health Advisories Tables*; Washington, DC, 2018.
[10] Zhang, R.; Liu, B.; Ma, J.; Zhu, R. Preparation and characterization of carboxymethyl cellulose/chitosan/alginic acid hydrogels with adjustable pore structure for adsorption of heavy metal ions. *Eur. Polym. J*. **2022,** *179*, 111577.
[11] Shrestha, R.; Ban, S.; Devkota, S.; Sharma, S.; Joshi, R.; Tiwari, A. P.; Kim, H. Y.; Joshi, M. K. Technological trends in heavy metals removal from industrial wastewater: A review. *J. Environ. Chem. Eng*. **2021,** *9*, 105688.
[12] Wang, Q.; Yu, J.; Chen, X. Y.; Du, D.; Wu, R.; Qu, G.; Guo, X.; Jia, H.; Wang, T. Non-thermal plasma oxidation of Cu (II)-EDTA and simultaneous Cu (II) elimination by chemical precipitation. *J. Environ. Manage*. **2019,** *248*, 109237.
[13] Yan, R.; Luo, D.; Fu, C.; Wang, Y.; Zhang, H.; Wu, P.; Jiang, W. Harmless treatment and selective recovery of acidic Cu (II)-Cr (VI) hybrid wastewater via coupled photo-reduction and ion exchange. *Sep. Purif. Technol*. **2020,** *234*, 116130.
[14] Saleem, H.; Pal, P.; Haija, M. A.; Banat, F. Regeneration and reuse of bio-surfactant to produce colloidal gas aphrons for heavy metal ions removal using single and multistage cascade flotation. *J. Clean. Prod*. **2019,** *217*, 493-502.
[15] Vo, T. S.; Hossain, M. M.; Jeong, H. M.; Kim, K. Heavy metal removal applications using adsorptive membranes. *Nano. Converg*. **2020,** *7*, 36.

[16] Kuang, Y.; Zhang, Z.; Wu, D. Synthesis of graphene oxide/polyethyleneimine sponge and its performance in the sustainable removal of Cu (II) from water. *Sci. of the Total Environ*. **2022,** *806*, 151258.
[17] Gu, Q.; Ng, T. C. A.; Bao, Y.; Ng, H. Y.; Tan, S. C.; Wang, J. Developing better ceramic membranes for water and wastewater treatment: where microstructure integrates with chemistry and functionalities. *J. Chem. Eng*. **2021,** *428*, 130456.
[18] Efome, J. E.; Rana, D.; Matsuura, T.; Lan, C. Q. Experiment and modeling for flux and permeate concentration of heavy metal ion in adsorptive membrane filtration using a metal-organic framework incorporated nanofibrous membrane. *J. Chem. Eng*. **2018,** *352*, 737-744.
[19] Siddiqui, S.; Surananai, S.; Sainath, K.; Zubair Khan, M.; Raja Pandiyan Kuppusamy, R.; Kempaiah Suneetha, Y. Emerging trends in development and application of 3D printed nanocomposite polymers for sustainable environmental solutions. *Eur. Polym. J*. **2023,** *196*, 112298.
[20] Ramos-Jacques, A. L.; Lujan-Montelongo, J. A.; Silva-Cuevas, C.; Cortez-Valadez, M.; Estevez, M.; Hernandez-Martínez, A. R. Lead (II) removal by poly(N,N-Dimethylacrylamide-Co-2-Hydroxyethyl Methacrylate). *Eur. Polym. J*. **2018,** *101*, 262-272.
[21] Guo, Q.; Xu, M.; Tang, Q.; Liu, Y.; Zhang, W.; Guo, C.; Zhao, X.; Zhu, Y.; Ye, S.; Liu, D.; Lei, W.; Chen, C. Advanced hybrid nanosheet membranes with stable nanochannels for ultrafast molecular separation. *NPJ Clean Water* **2023,** *6*, 38.
[22] Geng, W.; Zhang, Z.; Guo, Q.; Liu, Y.; Ye, X.; Zhang, H.; Fu, C.; Liu, F.; Zhu, Y.; Chen, C. Tailoring graphene oxide nanofiltration membrane with adjustable nanochannels for enhanced molecule separation. *J. Chem. Eng*. **2023,** *478*, 147327.
[23] Liu, Y.; Tang, Q.; Xu, M.; Ren, J.; Guo, C.; Chen, C.; Geng, W.; Lei, W.; Zhao, X.; Liu, D. Efficient mechanical exfoliation of mxene nanosheets. *J. Chem. Eng*. **2023,** *468*, 143439.
[24] Jalvo, B.; Aguilar-Sanchez, A.; Ruiz-Caldas, M. X.; Mathew, A. P. Water filtration membranes based on non-woven cellulose fabrics: effect of nanopolysaccharide coatings on selective particle rejection, antifouling, and antibacterial properties. *Nanomaterials* **2021,** *11*, 1752.
[25] Yanar, N.; Yang, E.; Park, H.; Son, M.; Choi, H. Efficacy of electrically-polarized 3D printed graphene-blended spacers on the flux enhancement and scaling resistance of water filtration membranes. *ACS Sustain. Chem. Eng*. **2021,** *9*, 6623-6631.
[26] Pagno, V.; Módenes, A. N.; Dragunski, D. C.; Fiorentin-Ferrari, L. D.; Caetano, J.; Guellis, C.; Goncąlves, B. C.; Dos Anjos, E. V.; Pagno, F.; Martinelli, V. Heat treatment of polymeric PBAT/PCL membranes containing activated carbon from brazil nutshell biomass obtained by electrospinning and applied in drug removal. *J. Environ. Chem. Eng*. **2020,** *8*, 104159.
[27] Intachai, S.; Na Nakorn, M.; Kaewnok, A.; Pankam, P.; Sumanatrakul, P.; Khaorapapong, N. Versatile inorganic adsorbent for efficient and practical removal of hexavalent chromium in water. *Mater. Chem. Phys*. **2022,** *288*, 126388.
[28] Morcos, G. S.; Ibrahim, A. A.; El-Sayed, M. M. H.; El-Shall, M. S. High performance functionalized UiO metal organic frameworks for the efficient and selective adsorption of Pb (II) ions in concentrated multi-ion systems. *J. Environ. Chem. Eng*. **2021,** *9*, 105191.
[29] Chen, Z.; Xu, C.; Hu, G.; Zhang, L.; Liu, Y.; Zhang, X.; Wu, S.; Hu, W.; Wang, Z.; Wei, Y. Selective removal of $Sr2^{+}$ by cation exchange using silica-based titanate adsorbents. *J. Solid. State. Chem*. **2022,** *312*, 123247.
[30] Geroeeyan, A.; Niazi, A.; Konoz, E. Removal of basic orange 2 dye and Ni^{2+} from aqueous solutions using alkaline-modified nanoclay. *Water Sci. and Tech*. **2021,** *83*, 2271-2286.
[31] Mohajeri, P.; Smith, C. M. S.; Chau, H. W.; Lehto, N.; Azimi, A.; Farraji, H. Adsorption behavior of Na-bentonite and nano cloisite Na^{+} in interaction with $Pb(NO_3)_2$ and $Cu(NO_3)_2{\cdot}3H_2O$ contamination in landfill liners: optimization by response surface methodology. *J. Environ. Chem. Eng*. **2019,** *7*, 103449.
[32] Msaadi, R.; Ammar, S.; Chehimi, M. M.; Yagci, Y. Diazonium-based ion-imprinted polymer/clay nanocomposite for the selective extraction of lead (II) ions in aqueous media. *Eur. Polym. J*. **2017,** *89*, 367-380.
[33] Wang, G.; Ding, C.; Liu, N.; Liu, H.; Yang, J.; Ma, S.; He, C.; Zhao, H. Complexant-montmorillonite nanocomposites for heavy metal binding in sulfide tailing. *J. Mat. Res. Tec.* **2022,** *17*, 329-341.
[34] Maric, T.; Nasir, M. Z. M.; Mayorga-Martinez, C. C.; Rosli, N. F.; Budanović, M.; Szökölová, K.; Webster, R. D.; Sofer, Z.; Pumera, M. Cloisite microrobots as self-propelling cleaners for fast and efficient removal of improvised organophosphate nerve agents. *ACS Appl. Mater. Interfaces* **2019,** *11*, 31832-31843.
[35] Zanini, N. C.; Ferreira, R. R.; Barbosa, R. F. S.; de Souza, A. G.; Camani, P. H.; Oliveira, S. A.; Mulinari, D. R.; Rosa, D. S. Two different routes to prepare porous biodegradable composite membranes containing nanoclay. *J.*

Appl. Polym. Sci. **2023,** *140*, e54630.
[36] Barbosa, R. F. S.; Zanini, N. C.; Mulinari, D. R.; Rosa, D. S. Hexavalent chromium sorption by modified cellulose macro and nanofibers obtained from eucalyptus residues. *J. Polym. Environ*. **2022,** *30*, 3852-3864.
[37] Hidayat, N.; Suhartini, S.; Arinda, T.; Elviliana, E.; Melville, L. Literature review on ability of agricultural crop residues and agro-in-dustrial waste for treatment of wastewater. *Int. J. Recycl. Org. Waste Agric.* **2022,** *11*, 553-585.
[38] Haripriyan, U.; Gopinath, K. P.; Arun, J. Chitosan based nano adsorbents and its types for heavy metal removal: A mini review. *Mater. Lett*. **2022,** *312*, 131670.
[39] Huang, Y.; Xiao, J.; Shi, C.; Li, M.; Ren, B.; Liu, Z.; Qi, Y. Bifunctional core-shell structure NaA zeolite@ mesoporous-silica/curcumin nanocomplexes for removing heavy metals and reduction of cadmium-induced damage. *Microporous Mesoporous Mater*. **2022,** *345*, 112262.
[40] Moradi, G.; Zinadini, S.; Rajabi, L.; Ashraf Derakhshan, A. Removal of heavy metal ions using a new high performance nanofiltration membrane modified with curcumin boehmite nanoparticles. *J. Chem. Eng*. **2020,** *390*, 124546.
[41] Yixuan, L.; Qaria, M. A.; Sivasamy, S.; Jianzhong, S.; Daochen, Z. Curcumin production and bioavailability: A comprehensive review of curcumin extraction, synthesis, biotransformation and delivery systems. *Ind. Crops. Prod*. **2021,** *172*, 114050.
[42] Xi, W.; Zhai, J.; Tian, L.; Zhou, S.; Zhang, Z. Curcumin-$Cu2^{+}$ complex generated on carbon nanotubes for electrocatalytic application toward electrooxidation of hydroxylamine. *Microchem. J*. **2021,** *161*, 105792.
[43] Ferrari, E. Chapter 15-Curcumin derivatives as metal-chelating agents: implications for potential therapeutic agents for neurological disorders. In *Curcumin for Neurological and Psychiatric Disorders*; Farooqui T., Farooqui A. A. B. T. C., Farooqui N., Farooqui P. D., Eds.; AP, 2019; pp 275-299.
[44] Moradi, G.; Zinadini, S.; Rajabi, L.; Ashraf Derakhshan, A. Removal of Heavy metal ions using a new high performance nanofiltration membrane modified with curcumin boehmite nanoparticles. *J. Chem. Eng*. **2020,** *390*, 124546.
[45] Hashim, A. F.; Youssef, K.; Roberto, S. R.; Abd-Elsalam, K. A. Chapter 3-Hybrid inorganic-polymer nanocomposites: synthesis, characterization, and plant-protection applications. In *Multifunctional Hybrid Nanomaterials for Sustainable Agri-Food and Ecosystems*; Abd-Elsalam K. A., Ed.; Elsevier, 2020; pp 33-49.
[46] Jha, E.; Panda, P. K.; Patel, P.; Kumari, P.; Mohanty, S.; Parashar, S. K. S.; Ahuja, R.; Verma, S. K.; Suar, M. Intrinsic atomic interaction at molecular proximal vicinity infer cellular biocompatibility of antibacterial nanopepper. *Nanomedicine* **2021,** *16*, 307-322.
[47] de Oliveira, S. A.; Camani, P. H.; da Silva Barbosa, R. F.; Rocha, D. B.; Mitra, S. K.; dos Santos Rosa, D. PBAT-based microfiltration membranes using porogen saturated solutions: architecture, morphology, and environmental profile. *J. Polym. Environ*. **2021,** *30*, 270-294.
[48] Jenkins, S. H. Waste discharge into the marine environment. Principles and guidelines for the Mediterranean action plan. *Marine Pollution Bulletin* **1983,** *14*, 76-76.
[49] Salehi, E.; Madaeni, S. S. Influence of poly (ethylene glycol) as pore-generator on morphology and performance of chitosan/poly (vinyl alcohol) membrane adsorbents. *Appl. Surf. Sci.* **2014,** *288*, 537-541.
[50] Barbosa, R. F. S.; Zanini, N. C.; Mulinari, D. R.; Rosa, D. S. Hexavalent chromium sorption by modified cellulose macro and nanofibers obtained from eucalyptus residues. *J. Polym. Environ*. **2022,** *30*, 3852-3864.
[51] Rada, S.; Dehelean, A.; Culea, E. FTIR, Raman, and UV-Vis spectroscopic and DFT investigations of the structure of iron-lead-tellurate glasses. *J. Mol. Model*. **2010,** *17*, 2103-2111.
[52] Sato, Y.; Hayami, R.; Yamamoto, K.; Gunji, T. Syntheses and properties of Cu (II), Al (III), and Ti (IV) coordination polymers using an acetylacetonato-terminated polyhedral oligomeric silsesquioxane. *Polym. J.* **2022,** *54*, 985-993.
[53] Zdiri, K.; Elamri, A.; Hamdaoui, M. Advances in thermal and mechanical behaviors of PP/clay nanocomposites. *Polymer-plastics technology and engineering* **2017,** *56*, 824-840.
[54] Zhang, Q.; Polyakov, N. E.; Chistyachenko, Y. S.; Khvostov, M. V.; Frolova, T. S.; Tolstikova, T. G.; Dushkin, A. V.; Su, W. Preparation of curcumin self-micelle solid dispersion with enhanced bioavailability and cytotoxic activity by mechanochemistry. *Drug. Deliv*. **2018,** *25*, 198-209.
[55] Jha, E.; Panda, P. K.; Patel, P.; Kumari, P.; Mohanty, S.; Parashar, S. K. S.; Ahuja, R.; Verma, S. K.; Suar, M. Intrinsic atomic interaction at molecular proximal vicinity infer cellular biocompatibility of antibacterial nanopepper. *Nanomedicine* **2021,** *16*, 307-322.
[56] Said, Z.; Cakmak, N. K.; Sharma, P.; Sundar, L. S.; Inayat, A.; Keklikcioglu, O.; Li, C. Synthesis, stability, density,

viscosity of ethylene glycol-based ternary hybrid nanofluids: experimental investigations and model-prediction using modern machine learning techniques. *Powder. Technol*. **2022,** *400*, 117190.
[57] Resner, L.; Lesiak, P.; Taraghi, I.; Kochmanska, A.; Figiel, P.; Piesowicz, E.; Zenker, M.; Paszkiewicz, S. Polymer hybrid nanocomposites based on homo and copolymer xlpe containing mineral nanofillers with improved functional properties intended for insulation of submarine cables. *Polymers* **2022,** *14*, 3444.
[58] Banerjee, R.; Ray, S. S.; Ghosh, A. K. Rheology and foaming behaviour of styrene-ethylene-butylene-styrene nanocomposites. *Colloid Polym. Sci*. **2021,** *299*, 481-496.
[59] Abdolrsaouli, M. H.; Babaei, A.; Kaschta, J.; Nazockdat, H. Polylactide/organoclay nanocomposites: The effect of organoclay types on the structure development and the kinetic of cold crystallization. *J. Vinyl Addit. Techn.* **2019,** *25*, 48-58.
[60] Sinha Ray, S.; Pouliot, S.; Bousmina, M.; Utracki, L. A. Role of organically modified layered silicate as an active interfacial modifier in immiscible polystyrene/polypropylene blends. *Polymer* **2004,** *45*, 8403-8413.
[61] Garcíaa, S. L.; Sánchez-Valdésb, S.; Ramos-Devallec, L. F. Effect of type and concentration of ionomer compatibilizer on the HDPE/Ionomer/Clay nanocomposites morphology. *Materials Science Forum* **2010,** *644*, 17-20.
[62] Hatami, M.; Dehghan, A.; Djafarzadeh, N. Investigations of addition of low fractions of nanoclay/latex nanocomposite on mechanical and morphological properties of cementitious materials. *Arab. J. Chem*. **2018,** *11*, 970-980.
[63] Andrade-Guel, M.; Cabello-Alvarado, C.; Romero-Huitzil, R. L.; Rodríguez-Fernández, O. S.; Ávila-Orta, C. A.; Cadenas-Pliego, G.; Medellín-Banda, D. I.; Gallardo-Vega, C.; Cepeda-Garza, J. Nanocomposite PLA/C20A nanoclay by ultrasound-assisted melt extrusion for adsorption of uremic toxins and methylene. *Nanomaterials* **2021,** *11*, 1-21.
[64] Patiño-Soto, A. P.; Sanchez-Valdes, S.; Ramos-Devalle, L. F. Morphological and thermal properties of ABS/montmorillonite nanocomposites using two different abs polymers and four different montmorillonite clays. *J. Polym. Sci. B: Polym. Phys.* **2007,** *46*, 190-200.
[65] Aparicio, P.; Galán, E. Mineralogical interference on kaolinite crystallinity index measurements. *Clays. Clay. Miner*. **1999,** *47*, 12-27.
[66] Kiyani, M. M.; Sohail, M. F.; Shahnaz, G.; Rehman, H.; Akhtar, M. F.; Nawaz, I.; Mahmood, T.; Manzoor, M.; Bokhari, S. A. I. Evaluation of turmeric nanoparticles as anti-gout agent: modernization of a traditional drug. *Medicina* **2019,** *55*, 1-11.
[67] Poggere, G. C.; Melo, V. F.; Francelino, M. R.; Simas, F. N. B.; Schaefer, C. E. G. R. Adsorption of arsenate ($HAsO_4^{2-}$) by the clay fraction of soils of the keller and barton peninsulas, king george island, maritime antarctic. *Rev. Cienc. Agron*. **2017,** *48*, 13-21.
[68] Vo, T. G.; Ho, P. Y.; Chiang, C. Y. Operando mechanistic studies of selective oxidation of glycerol to dihydroxyacetone over amorphous cobalt oxide. *Appl. Catal. B: Environ*. **2022,** *300*, 120723.
[69] Ferreira, R. R.; Souza, A. G.; Nunes, L. L.; Shahi, N.; Rangari, V. K.; Rosa, D. S. Use of ball mill to prepare nanocellulose from eucalyptus biomass: challenges and process optimization by combined method. *Mater. Today Commun*. **2020,** *22*, 100755.
[70] Qiu, W.; Vakili, M.; Cagnetta, G.; Huang, J.; Yu, G. Effect of high energy ball milling on organic pollutant adsorption properties of chitosan. *Int. J. Biol. Macromol*. **2020,** *148*, 543-549.
[71] Li, R.; Rao, D.; Zhou, J.; Wu, G.; Wang, G.; Zhu, Z.; Han, X.; Sun, R.; Li, H.; Wang, C.; Yan, W.; Zheng, X.; Cui, P.; Wu, Y.; Wang, G.; Hong, X. Amorphization-induced surface electronic states modulation of cobaltous oxide nanosheets for lithium-sulfur batteries. *Nat. Commun*. **2021,** *12*, 6-13.
[72] Vakili, M.; Qiu, W.; Cagnetta, G.; Huang, J.; Yu, G. Solvent-free mechanochemical mild oxidation method to enhance adsorption properties of chitosan. *Front. Environ. Sci. Eng*. **2021,** *15*, 1-14.
[73] Mohamed, S. A.; Kim, J. Gas adsorption enhancement in partially amorphized metal-organic frameworks. *The Journal of Physical Chemistry C* **2021,** *125*, 4509-4518.
[74] Reyes-Gasga, J.; Koudriavtseva, O.; Herrera-Becerra, R.; Escobosa, A. XRD characterization of crystallinity of human tooth enamel under influence of mechanical grinding. *Mater. Sci. and App*. **2015,** *6*, 464-472.
[75] Joly, A.; Latha, M. S. Synthesis of nanocurcumin-alginate conjugate and its characterization by XRD, IR, UV-VIS andraman spectroscopy. *Orient. J. Chem*. **2019,** *35*, 751-756.
[76] El-Rahman, S. N. A.; Al-Jameel, S. S. Protection of curcumin and curcumin nanoparticles against cisplatin induced nephrotoxicity in male rats. *Sch. Acad. J. Biosci*. **2014,** *2*, 214-223.
[77] Li, X.; Tan, D.; Xie, L.; Sun, H.; Sun, S.; Zhong, G.; Ren, P. Effect of surface property of halloysite on the

crystallization behavior of PBAT. *Appl. Clay. Sci*. **2018,** *157*, 218-226.
[78] Garalde, R. A.; Thipmanee, R.; Jariyasakoolroj, P.; Sane, A. The effects of blend ratio and storage time on thermoplastic starch/poly (butylene adipate-co-terephthalate) films. *Heliyon* **2019,** *5*, e01251.
[79] Moustafa, H.; Guizani, C.; Dufresne, A. Sustainable biodegradable coffee grounds filler and its effect on the hydrophobicity, mechanical and thermal properties of biodegradable PBAT composites. *J. Appl. Polym. Sci*. **2017,** *134*, 44498.
[80] Kashi, S.; Gupta, R. K.; Kao, N.; Hadigheh, S. A.; Bhattacharya, S. N. Influence of graphene nanoplatelet incorporation and dispersion state on thermal, mechanical and electrical properties of biodegradable matrices. *J. Mater. Sci. Technol*. **2018,** *34*, 1026-1034.
[81] Andrade, M. F. C.; Loureiro, H. C.; Sarantopóulos, C. I. G. L.; Morales, A. R. Blends of poly (butylene adipate-co-terephthalate) and thermoplastic whey protein isolate: A compatibilization study. *J. Polym. Environ*. **2021,** *29*, 3288-3301.
[82] Camani, P. H.; Toguchi, J. P. M.; Fiori, A. P. S. M.; Rosa, D. S. Impact of unmodified (PGV) and modified (Cloisite 20A) nanoclays into biodegradability and other properties of (bio) nanocomposites. *Appl. Clay. Sci*. **2020,** *186*, 105453.
[83] Pal, A. K.; Wu, F.; Misra, M.; Mohanty, A. K. Reactive extrusion of sustainable PHBV/PBAT-based nanocomposite films with organically modified nanoclay for packaging applications: compression moulding vs. cast film extrusion. *Compos. Part B: Eng*. **2020,** *198*, 108-141.
[84] Barbosa, R. F. S.; Oliveira, S.; Souza, A. G.; Rosa, D. Development of biodegradable membranes with incorporation of cellulose nanostructure for water treatment. *Conference: Congresso Brasileiro de Polímeros*; Bento Gonçalves, 2019; pp 1985-1989.
[85] Totsche, K. U.; Amelung, W.; Gerzabek, M. H.; Guggenberger, G.; Klumpp, E.; Knief, C.; Lehndorff, E.; Mikutta, R.; Peth, S.; Prechtel, A.; Ray, N.; Kögel-Knabner, I. Microaggregates in soils. *J. Pla. Nutri. So. Sci*. **2018,** *181*, 104-136.
[86] Liu, M.; Sun, J.; Sun, Y.; Bock, C.; Chen, Q. Thickness-dependent mechanical properties of polydimethylsiloxane membranes. *J. Micromech. Microeng*. **2009,** *19*, 035028.
[87] Lima, E. P. N.; Galdino, T. P.; Farias, R. Í. R.; Melo, I. G.; Queiroz, S. F. A. M.; Santos, A. C. Q.; Fook, M. V. L. Influence of thickness on the mechanical properties, contact angle, absorption, and loss in water of membrane from natural latex. *Matéria (Rio de Janeiro)* **2021,** *26*, e13077.
[88] Cai, Y.; Lv, J.; Feng, J. Spectral characterization of four kinds of biodegradable plastics: poly (lactic acid), poly (butylenes adipate-co-terephthalate), poly (hydroxybutyrate-co-hydroxyvalerate) and poly (butylenes succinate) with FTIR and raman spectroscopy. *J. Polym. Environ*. **2013,** *21*, 108-114.
[89] Barbosa, R. F. S.; Souza, A. G.; Rosa, D. S. Acetylated cellulose nanostructures as reinforcement materials for PBAT nanocomposites. *Polym. Compos*. **2020,** *41*, 2841-2854.
[90] Almutairi, F. M.; El Rabey, H. A.; Tayel, A. A.; Alalawy, A. I.; Al-Duais, M. A.; Sakran, M. I.; Zidan, N. S. Augmented anticancer activity of curcumin loaded fungal chitosan nanoparticles. *Int. J. Biol. Macromol*. **2020,** *155*, 861-867.
[91] Moghaddasi, F.; Housaindokht, M. R.; Darroudi, M.; Bozorgmehr, M. R.; Sadeghi, A. Synthesis of nano curcumin using black pepper oil by O/W nanoemulsion technique and investigation of their biological activities. *LWT-Food Science and Technology* **2018,** *92*, 92-100.
[92] Silva, M. C.; Nascimento, I.; Ribeiro, V. S.; Fook, M. V. L. Evaluation of the obtaining method of chitosan/curcumin scaffolds on the structure, morphology and thermal properties. *Rev. Mater*. **2016,** *21*, 560-568.
[93] De Souza Ferreira, S. B.; Bruschi, M. L. Improving the bioavailability of curcumin: Is micro/nanoencapsulation the key? *Ther. Deliv*. **2019,** *10*, 83-86.
[94] Raj, S.; Shankaran, D. R. Curcumin based biocompatible nanofibers for lead ion detection. *Sens. Actuators B: Chem*. **2016,** *226*, 318-325.
[95] Naderi-Samani, H.; Shoja Razavi, R.; Loghman-Estarki, M. R.; Ramazani, M. The effects of organoclay on the morphology and mechanical properties of PAI/clay nanocomposites coatings prepared by the ultrasonication assisted process. *Ultrason Sonochem* **2017,** *38*, 306-316.
[96] Raji, M.; Essassi, E.; Essabir, H.; Rodrigue, D.; Qaiss, A. E. K.; Bouhfid, R. Properties of nano-composites based on different clays and polyamide 6/acrylonitrile butadiene styrene blends. In *Bio-based Polymers and Nanocomposites: Preparation, Processing, Properties & Performance*; Sanyang M. L., Jawaid M., Eds.; Springer International Publishing: Cham, 2019; pp 107-128.
[97] Correia, P. R. C.; Santana, J. S.; Ramos, I. G.; Sant'Ana, A. E. G.; Goulart, H. F.; Druzian, J. I. Development of

membranes composed of poly (butylene adipate-co-terephthalate) and activated charcoal for use in a controlled release system of pheromone. *J. Polym. Environ*. **2019,** *27*, 1781-1789.
[98] Ludwiczak, J.; Frąckowiak, S.; Leluk, K. Study of thermal, mechanical and barrier properties of biodegradable PBAT/PBAT films with highly oriented MMT. *Materials* **2021,** *14*, 7189.
[99] Xing, Y.; Zhang, Y.; Ding, S.; Zheng, X.; Xu, M.; Cao, Y.; Gui, X. Effect of surface roughness on the detachment between bubble and glass beads with different contact angles. *Powder Technol*. **2020,** *361*, 812-816.
[100]Islam, A.; Yasin, T.; Sabir, A.; Khan, S. M.; Sultan, M.; Shafiq, M.; Khan, A. U.; Jamil, T. High-temperature electrical properties of silane cross-linked chitosan/poly (vinyl alcohol) membrane: thermal, mechanical and surface characterization. *E-Polymers* **2015,** *15*, 255-261.
[101]Lin, X.; Fan, X.; Li, R.; Li, Z.; Ren, T.; Ren, X.; Huang, T. S. Preparation and characterization of PHB/PBAT-based biodegradable antibacterial hydrophobic nanofibrous membranes. *Polym. Adv. Technol*. **2018,** *29*, 481-489.
[102]Aisueni, F.; Abunumah, O.; Hashim, I.; Ramalan, M.; Ogoun, E.; Prabhu, R.; Giwa, A.; Gobina, E. Effect of pore size and porosity on contact angle of ceramic membrane for oil-in-water emulsion separation. *TechConnect Briefs 2022*; Washington, USA, 2022.
[103]Botta, L.; Teresi, R.; Titone, V.; Salvaggio, G.; La Mantia, F. P.; Lopresti, F. Use of biochar as filler for biocomposite blown films: structure-processing-properties relationships. *Polymers* **2021,** *13*, 3953.
[104]Wang, X.; Gao, Y. Effects of length and unsaturation of the alkyl chain on the hydrophobic binding of curcumin with tween micelles. *Food Chem*. **2018,** *246*, 242-248.
[105]Kumar, P.; Sandeep, K. P.; Alavi, S.; Truong, V. D.; Gorga, R. E. Effect of type and content of modified montmorillonite on the structure and properties of bio-nanocomposite films based on soy protein isolate and montmorillonite. *J. Food Sci*. **2010,** *75*, N46-N56.
[106]Fukushima, K.; Rasyida, A.; Yang, M. C. Biocompatibility of organically modified nanocomposites based on PBAT. *J. Polym. Res*. **2013,** *20*, 302.
[107]Chen, J. H.; Chen, C. C.; Yang, M. C. Characterization of nanocomposites of poly (butylene adipate-co-terephthalate) blending with organoclay. *J. Polym. Res*. **2011,** *18*, 2151-2159.
[108]Roy, S.; Priyadarshi, R.; Ezati, P.; Rhim, J. W. Curcumin and its uses in active and smart food packaging applications-A comprehensive review. *Food Chem*. **2022,** *375*, 131885.
[109]Shi, L.; Kang, L.; Gong, J.; Zhang, X.; Liao, J.; Mo, L.; Li, J. Cellulose nanofibrils reinforced films without chemical modification, hydrophobic, high elongation, and foldability. *Ind. Crops. Prod*. **2022,** *180*, 114742.
[110]Silva, M. A.; Freitas, C. M.; Xavier, D. R.; Romão, A. R. Sobreposição de riscos e impactos no desastre da vale em brumadinho. *Cienc. Cult*. **2020,** *72*, 21-28.
[111]Shajahan, A.; Shankar, S.; Sathiyaseelan, A.; Narayan, K. S.; Narayanan, V.; Kaviyarasan, V.; Ignacimuthu, S. Comparative studies of chitosan and its nanoparticles for the adsorption efficiency of various dyes. *Int. J. Biol. Macromol*. **2017,** *104*, 1449-1458.
[112]Gaikwad, R. W.; Sapkal, R. S.; Sapkal, V. S. Removal of copper ions from acid mine drainage wastewater using ion exchange technique: factorial design analysis. *J. Water Resour. Prot*. **2010,** *2*, 984-989.
[113]Xu, K.; Li, L.; Huang, Z.; Tian, Z.; Li, H. Efficient adsorption of heavy metals from wastewater on nanocomposite beads prepared by chitosan and paper sludge. *Sci. Total Env*. **2022,** *846*, 157399.
[114]Upadhyay, U.; Sreedhar, I.; Singh, S. A.; Patel, C. M.; Anitha, K. L. Recent advances in heavy metal removal by chitosan based adsorbents. *Carbohydr. Polym*. **2021,** *251*, 117000.
[115]Karimi, H. Effect of PH and initial pb (II) concentration on the lead removal efficiency from industrial wastewater using $Ca(OH)_2$. *Inter. J. Water and Wastewater Treat*. **2017,** *3*, 1-4.
[116]Kumar, A.; Balouch, A.; Pathan, A. A.; Jagirani, M. S.; Mahar, A. M.; Zubair, M.; Laghari, B. Remediation of nickel ion from wastewater by applying various techniques: A review. *Acta. Chemica. Malaysia.* **2019,** *3*, 1-15.